MPC for simultaneous electrical and thermal flow optimization in buildings

Shahriar Dadras Javan * **Benedikt Lammersmann** *
Martin Mönnigmann *

* *Automatic Control and Systems Theory, Ruhr-Universität Bochum, Germany*
(e-mail: Shahriar.DadrasJavan@ruhr-uni-bochum.de)

Abstract: We use model predictive control (MPC) for the optimal energy distribution in non-residential buildings. Our approach is special in that it treats thermal and electrical energy flows simultaneously. Our sample application is a real office building, where components such as heat pumps and heating rods introduce discrete variables. This implies the optimal control problem that must be solved for MPC is a mixed-integer quadratic programming (MIQP) problem. Because both continuous and integer variables are involved, the computation times may become prohibitive for use in real-time. We explore a computationally efficient approximation that replaces integer variables by continuous variables for later time steps along the horizon. The performance of MPC using this method is investigated in simulations and the results are compared to those for the original MIQP problem and solution. Our method significantly reduces computational time while achieving a nearly optimal solution.

Keywords: model predictive control, mixed-integer programming, computationally efficient, control applications, energy flows

1. INTRODUCTION

Buildings play a significant role in global energy consumption, and improving their energy efficiency is crucial for reducing CO_2 emissions. While Aghemo et al. (2013) point out that most contemporary buildings employ basic rule-based control (RBC) systems offering minimal energy savings, Killian and Kozek (2016) highlight model predictive control (MPC) potentials for energy management in buildings. With its capacity to balance multiple optimization goals, integrate predictions, and conform to operational constraints, MPC is identified as a highly suitable solution for enhancing energy efficiency of buildings.

MPC is computationally intensive, as it requires solving an optimal control problem (OCP) at every discrete time step. The introduction of discrete decision variables typically increases the complexity of the problem dramatically (see, e.g., Yao and Shekhar, 2021). This is relevant for building energy systems where devices like heat pumps and heating rods operate in discrete states, requiring the solution of mixed integer quadratic programming (MIQP) optimization problems. Cagienard et al. (2007) proposed move blocking strategies to mitigate the computational load by maintaining constant inputs at defined steps over the control horizon. Löhr et al. (2020) established an approach that involves an offline training phase for MIQP using machine learning techniques, paving the way for a faster and more practical online computations, though this comes with a trade-off in terms of result precision. For a comprehensive overview of MPC methodologies augmented with artificial neural networks, Afram et al. (2017) provides a detailed review. Löhr and Mönnigmann (2021) employed post-processing of continuous decision variables to ensure constraint satisfaction with heuristic rules. Our approach simplifies the MIQP by keeping discrete decision variables for the first steps along the horizon and using continuous variables for subsequent steps. This method decreases computational demands while ensuring constraint satisfaction. The performance of the method is illustrated through simulations that optimize energy flows within an actual office building, using real-world measured data as a foundation.

In Section 2, we introduce the energy system model of the office building. Section 3 elaborates on the associated MPC formulation and our novel method. We present the results of our simulations, demonstrating the effectiveness of our approach in Section 4. A summary is stated in Section 5.

2. SYSTEM OUTLINE AND MODEL FRAMEWORK

We implement MPC in an actual office building energy system, integrating various electrical and thermal subcomponents to achieve coupled and simultaneous optimal operation. Detailed models for each component are explained in Sections 2.1 and 2.2. These individual models are combined to form a discrete-time system model suitable for MPC in Section 2.3. The model presented here is composed of blocks that are similar to those introduced by Löhr and Mönnigmann (2018), where, however, a residential building was treated. We revisit and extend the subsystem models presented in Löhr and Mönnigmann (2018) for use with the particular non-residential building treated here. An overview of the system can be seen in

⋆ Support by the German Federal Ministry of Education and Research under grant 01LY2201B is gratefully acknowledged

Fig. 1. Abbreviations used in Fig. 1 and throughout the paper are explained in Table 1.

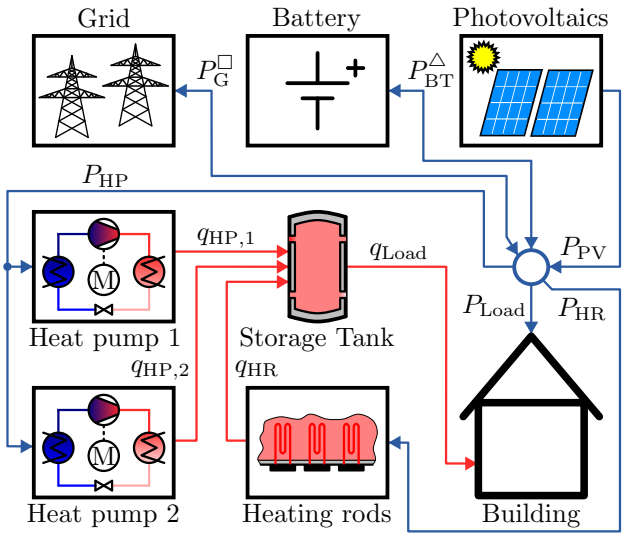

Fig. 1. Structure of heating and electrical system. Heat flows are illustrated by red lines, electrical flows are represented by blue lines. Bidirectional flows $P_{\mathrm{G}}^{\square}$, $\square \in \{\mathrm{dem}, \mathrm{sup}\}$ and $P_{\mathrm{BT}}^{\triangle}$, $\triangle \in \{\mathrm{ch}, \mathrm{dis}\}$ denote grid demand, grid supply, battery charging and battery discharging, respectively.

Table 1. List of index abbreviations

Abbreviation	Designation
G	Electric grid
BT	Electric battery
PV	Photovoltaics
HR	Heating rod
HP	Heat pump
ST	Hot water storage tank
Load	Load demand of the building
dem	Demand
sup	Supply
ch	Charging
dis	Discharging

2.1 Heating subsystem

The heating subsystem comprises two brine-to-water heat pumps, auxiliary electrical heating rods, and a hot water storage tank.

Heat pump Two brine-to-water heat pumps serve as the primary heat sources for charging the hot water storage tank. They can operate only in on/off modes and their functionality is modelled based on the relationship between the electrical input and the thermal output. The thermal flow of the heat pump i in sampling interval k is characterized by the time-dependent coefficient of performance (COP), denoted by $COP_i(k)$. This COP value depends on both the brine temperature and the supplied water temperature.
Let the heat pump efficiency be integrated into $COP_i(k)$, and $P_{\mathrm{HP},i}$ be the electrical power input of the heat pump i. The thermal flow of the heat pump i at time step k can be calculated from

$$q_{\mathrm{HP},i}(k) = COP_i(k) \cdot P_{\mathrm{HP},i}(k). \tag{1}$$

Since the two heat pumps are identical, the total heat flow they produce is given by

$$q_{\mathrm{HP}}(k) = \kappa(k)\, q_{\mathrm{HP}_0}(k), \tag{2}$$

where $\kappa(k) \in \{0, 1, 2\}$ is the number of heat pumps operating at time step k, and $q_{\mathrm{HP}_0}(k)$ is the heat flow generated by a single heat pump at time step k.

Heating rod Three heating rods, functioning in on/off modes, provide additional heat to charge the hot water storage tank. Since the three heating rods are identical, the cumulative heat flow they produce amounts to

$$q_{\mathrm{HR}}(k) = \lambda(k) \cdot q_{\mathrm{HR}_0}, \tag{3}$$

where $\lambda(k) \in \{0, 1, 2, 3\}$ indicates the number of operational heating rods at time step k, and q_{HR_0} designates the heat flow produced by a single active rod. The electrical power input for the operation of the heating rods with a 100 % efficiency read

$$q_{\mathrm{HR}}(k) = P_{\mathrm{HR}}(k). \tag{4}$$

Hot water storage tank The hot water storage tank is discharged to meet the heating requirements of the building. Using a simplified energy balance, the stored energy in the storage tank E_{ST} at time step $k+1$ is represented by

$$\begin{aligned} E_{\mathrm{ST}}(k+1) = {} & \alpha_1 E_{\mathrm{ST}}(k) + \beta_1 q_{\mathrm{HP}}(k) + \beta_2 q_{\mathrm{HR}}(k) \\ & - \beta_3 q_{\mathrm{Load}}(k), \end{aligned} \tag{5}$$

where $\alpha_1 E_{\mathrm{ST}}(k)$ represents the the stored energy of the hot water storage tank at time step k reduced by the loss factor α_1, q_{Load} denotes the thermal load drawn to meet the demand of the building, and β_i, $i \in \{1, 2, 3\}$ correspond to efficiencies. The stored energy is bounded from below and above according to

$$0 \leq E_{\mathrm{ST}}(k) \leq E_{\mathrm{ST}}^{\max}, \tag{6}$$

where the upper bound results from an upper bound on the hot water temperature.

2.2 Electrical subsystem

The electrical subsystem powers the electric elements of the heating system, and computer equipment and appliances (P_{Load}). It consists of a battery, photovoltaics units, and a grid connection.

Photovoltaics The photovoltaics power output can be presented by a linear model of global irradiation as

$$P_{\mathrm{PV}}(k) = \mu G(k), \tag{7}$$

where $G(k)$ denotes the global irradiation, and μ encompasses a factor that combines parameters associated with the physical properties and installation conditions of the photovoltaic units, as well as other relevant factors. We use real history data of the global irradiation of the building to fit a linear model and find μ.

Battery The energy balance of the battery reads

$$E_{\mathrm{BT}}(k+1) = \alpha_2 E_{\mathrm{BT}}(k) + \beta_4 P_{\mathrm{BT}}^{\mathrm{ch}}(k) - \beta_5 P_{\mathrm{BT}}^{\mathrm{dis}}(k), \tag{8}$$

where $\alpha_2 E_{\mathrm{BT}}(k)$ is the stored energy of the battery adjusted by the loss factor α_2, and $P_{\mathrm{BT}}^{\mathrm{ch}}(k)$ and $P_{\mathrm{BT}}^{\mathrm{dis}}(k)$ denote the electrical power flow into and out of the battery with efficiency factors β_4 and β_5. The energy stored in the battery is subject to the bounds

$$E_{\mathrm{BT}}^{\min} \leq E_{\mathrm{BT}}(k) \leq E_{\mathrm{BT}}^{\max}, \tag{9}$$

where the lower bound must be respected to avoid deep discharging.

Grid connection The grid connection can either demand power from the grid, labelled as $P_{\mathrm{G}}^{\mathrm{dem}}$, or supply power to the grid, referred to as $P_{\mathrm{G}}^{\mathrm{sup}}$.

Electrical balance node As the virtual balance node depicted in Fig. 1 cannot store energy, the total power entering and leaving the electrical node at each time step k are in balance, therefore

$$\begin{aligned} &P_{\mathrm{G}}^{\mathrm{dem}}(k) + \eta P_{\mathrm{BT}}^{\mathrm{dis}}(k) + \eta P_{\mathrm{PV}}(k) = P_{\mathrm{Load}}(k) \\ &+P_{\mathrm{G}}^{\mathrm{sup}}(k) + P_{\mathrm{HP}}(k) + P_{\mathrm{HR}}(k) + \tfrac{1}{\eta} P_{\mathrm{BT}}^{\mathrm{ch}}(k), \end{aligned} \tag{10}$$

where η is the AC to DC power conversion coefficient and vice versa of the battery inverter.

2.3 System Model

We regard stored energies as state variables, i.e., $x(k) = [E_{\mathrm{ST}}(k), E_{\mathrm{BT}}(k)]^T$, with thermal and electrical energy flows as inputs. Continuous and integer inputs are denoted by $u(k)$ and $\delta(k)$, respectively, to clearly distinguish them from one another. These inputs encompass

$$u(k) = \begin{bmatrix} P_{\mathrm{BT}}^{\mathrm{ch}}(k) \\ P_{\mathrm{BT}}^{\mathrm{dis}}(k) \\ P_{\mathrm{G}}^{\mathrm{dem}}(k) \\ P_{\mathrm{G}}^{\mathrm{sup}}(k) \end{bmatrix}, \delta(k) = \begin{bmatrix} \kappa(k) \\ \lambda(k) \end{bmatrix}. \tag{11}$$

The thermal loads are considered to be measured disturbances $d(k) = [q_{\mathrm{Load}}(k)]$. The resulting linear discrete-time state space model reads

$$\begin{aligned} x(k+1) &= Ax(k) + B_u u(k) + B_\delta \delta(k) + Ed(k) \\ y(k) &= Cx(k), \end{aligned} \tag{12}$$

with system matrices

$$A = \begin{bmatrix} \alpha_1 & 0 \\ 0 & \alpha_2 \end{bmatrix}, B_u = \begin{bmatrix} 0 & 0 & 0 & 0 \\ \beta_4 & -\beta_5 & 0 & 0 \end{bmatrix},$$

$$B_\delta = \begin{bmatrix} \beta_1 \cdot q_{\mathrm{HP}_0}(k) & \beta_2 \cdot q_{\mathrm{HR}_0} \\ 0 & 0 \end{bmatrix}, E = \begin{bmatrix} -\beta_3 \\ 0 \end{bmatrix}, \text{and } C = \begin{bmatrix} 1 & 0 \\ 0 & 1 \end{bmatrix}.$$

3. CONTROL STRATEGY

We solve an OCP identifying the optimal electrical and thermal flows in the system on a receding horizon. The model ensures thermal comfort by matching the discharge from the hot water storage tank to the demand of building at each time step as can be seen in (5). The subsequent subsections present the cost function, constraints, and the MPC problem statement.

3.1 Cost function

The cost function reads

$$J(k) = J_y(k) + J_u(k) + J_\delta(k), \tag{13}$$

where $J_y(k)$ models reference tracking for the target levels of the battery and the hot water storage tank, and $J_u(k)$ and $J_\delta(k)$ regulate continuous and discrete energy flows, respectively. Let $(*)(k+i|k)$ represent the prediction of variable $(*)$ for time step $k+i$ using information from time step k, for example $E_{\mathrm{BT}}(k+i|k)$ correspond to the prediction of the stored energy of the battery. Further let $r_{(*)}$ denote the tuning parameter adjusted for specific objectives linked with the variable $(*)$. The cost function terms then can be stated as

$$\begin{aligned} J_y(k) = \sum_{i=1}^{N} & r_{\mathrm{E,ST}}(k+i)(E_{\mathrm{ST}}^{\mathrm{ref}}(k+i) - E_{\mathrm{ST}}(k+i|k))^2 \\ &+ r_{\mathrm{E,BT}}(k+i)(E_{\mathrm{BT}}^{\mathrm{ref}}(k+i) - E_{\mathrm{BT}}(k+i|k))^2, \end{aligned} \tag{14a}$$

$$\begin{aligned} J_u(k) = \sum_{i=0}^{N-1} & r_{\mathrm{BT,ch}}(k+i)(P_{\mathrm{BT}}^{\mathrm{ch}}(k+i|k))^2 \\ &+ r_{\mathrm{BT,dis}}(k+i)(P_{\mathrm{BT}}^{\mathrm{dis}}(k+i|k))^2 \\ &+ r_{\mathrm{G,dem}}(k+i)(P_{\mathrm{G}}^{\mathrm{dem}}(k+i|k))^2 \\ &+ r_{\mathrm{G,sup}}(k+i)(P_{\mathrm{G}}^{\mathrm{sup}}(k+i|k))^2, \end{aligned} \tag{14b}$$

and

$$\begin{aligned} J_\delta(k) = \sum_{i=0}^{N-1} & r_\kappa(k+i)(\kappa(k+i|k))^2 \\ &+ r_\lambda(k+i)(\lambda(k+i|k))^2, \end{aligned} \tag{14c}$$

where N is the horizon.

Setting large $r_{\mathrm{E,ST}}$ and $r_{\mathrm{E,BT}}$ ensures closer adherence to the referenced levels of energy stored in the storage tank and battery. Setting large tuning parameters in (14b) and (14c), i.e., $r_{\mathrm{BT,ch}}$, $r_{\mathrm{BT,dis}}$, $r_{\mathrm{G,dem}}$, $r_{\mathrm{G,sup}}$, r_κ, and r_λ, serve to limit the corresponding continuous and integer energy flows, respectively. Assigning a higher value to r_λ than r_κ prioritizes the use of heat pumps over heating rods. This preference is advantageous, for example, because heat pumps are more efficient than heating rods.

3.2 Constraints

In addition to the constraints on the storage tank (6) and battery (9), the continuous inputs are subject to

$$0 \leq P_{j_1}^{j_2}(k) \leq P_{j_1}^{j_2,\max}(k), \tag{15}$$

$$\text{with } j_1 \in \{\mathrm{BT,G}\} \text{ and } j_2 \in \{\mathrm{ch,dis,dem,sup}\}, \tag{16}$$

where j_1 and j_2 refer to corresponding energy flows according to Table 1. The number of operational heat pumps and heating rods, represented by integer inputs, are subject to

$$\kappa(k) \in \{0,1,2\} \text{ and } \lambda(k) \in \{0,1,2,3\},$$

as integer constraints. Finally, to ensure the energy balance as outlined in (10), we use the associated set of inequality constraints

$$\begin{aligned} P_{\mathrm{HP}}(k) + P_{\mathrm{HR}}(k) + \frac{1}{\eta} P_{\mathrm{BT}}^{\mathrm{ch}}(k) + P_{\mathrm{G}}^{\mathrm{sup}}(k) \\ \leq -P_{\mathrm{Load}}(k) + \eta P_{\mathrm{BT}}^{\mathrm{dis}}(k) + P_{\mathrm{G}}^{\mathrm{dem}}(k), \\ -P_{\mathrm{HP}}(k) - P_{\mathrm{HR}}(k) - \frac{1}{\eta} P_{\mathrm{BT}}^{\mathrm{ch}}(k) - P_{\mathrm{G}}^{\mathrm{sup}}(k) \\ \leq P_{\mathrm{Load}}(k) - \eta P_{\mathrm{BT}}^{\mathrm{dis}}(k) - P_{\mathrm{G}}^{\mathrm{dem}}(k). \end{aligned} \tag{17}$$

3.3 Hybrid MPC

Collecting the cost function, the constraints and the system model yields the OCP

$$\min_{\substack{x(k+i_1|k)\\u(k+i_2|k)\\\delta(k+i_2|k)}} J(k) = J_y(k) + J_u(k) + J_\delta(k) \tag{18a}$$

$$\text{s.t.} \quad x(k+1) = Ax(k) + B_u u(k) + B_\delta \delta(k) + Ed(k), \\ y(k) = Cx(k), \tag{18b}$$

$$0 \le E_{\mathrm{ST}}(k+i_1|k) \le E_{\mathrm{ST}}^{\max}, \tag{18c}$$

$$0 \le E_{\mathrm{BT}}(k+i_1|k) \le E_{\mathrm{BT}}^{\max}, \tag{18d}$$

$$0 \le P_{j_1}^{j_2}(k+i_2|k) \le P_{j_1}^{j_2,\max}(k+i_2|k), \tag{18e}$$

$$\kappa(k+i_2|k) \in \{0,1,2\}, \tag{18f}$$

$$\lambda(k+i_2|k) \in \{0,1,2,3\}, \tag{18g}$$

$$(17), \tag{18h}$$

where all constraints must hold for all $i_1 \in \{1,2,\dots,N\}$, $i_2 \in \{0,1,\dots,N-1\}$, and the optimization variables are the variables stated underneath the min-operator for these indices. The indices j_1 and j_2 are used as explained for (16).

The OCP (18) can be cast into a standard MIQP form by introducing $\Xi(k) = [\xi(k|k), \xi(k+1|k), \dots, \xi(k+N-1|k)]$, where $\xi(k+i_2|k) = [u(k+i_2|k), \delta(k+i_2|k)]$ represents the combined predicted continuous and integer inputs at time step k. Using this augmented input and by substituting the dynamics (18b) into the cost function (18a) and constraints (18c-18h), the OCP can be transformed into a MIQP of the form

$$\begin{aligned} &\underset{\Xi(k)}{min}\ \Xi^T(k)\mathcal{H}(k)\Xi(k) - \mathcal{F}^T(k)\Xi(k) \\ &s.t. \qquad \Omega\Xi(k) \le \omega(k). \end{aligned} \tag{19}$$

The derivation of (19) is not elaborated here (see, e.g., Maciejowski and Huzmezan (2007) for further details).
Because (18) and (19) involve continuous and integer variables, their solution is computationally expensive. It is known that solving this problem can become prohibitively expensive for real-time embedded applications even for short horizons N (see Axehill and Hansson (2006) for numerical examples). We describe our approach to reducing this computational effort in the subsequent subsection.

3.4 Modified MIQP

Essentially, we split the horizon into a first part on which the mixed continuous-integer inputs are retained,

$$\{(k|k), (k+1|k), \dots, (k+i_s-1|k)\}, \tag{20a}$$

and a second part

$$\{(k+i_s|k), \dots, (k+N-1|k)\} \tag{20b}$$

where i_s, $1 \le i_s \le N$, refers to the time step at which the transition occurs. Reducing i_s results in a reduced computational effort for solving (18) or (19). Note that choosing i_s=1 still yields a solution that can readily be applied to the real system without having to convert any continuous variables to integer variables a posteriori.
We note that the relaxation of the integer variables to continuous variables does in general affect the stability properties of the closed-loop system. It is beyond the present paper to address this question from a theoretical perspective. We will investigate the behaviour in numerical experiments with data from a real building in the present paper.
We refer to the original problem with continuous and integer variables (19) as MIQP, and to the problem after introducing the splitting of the horizon (20) as modified MIQP (mMIQP) for short.

4. CASE STUDY AND SIMULATIONS

We analyse the performance of the proposed method by performing simulations utilizing actual data from a real office building. [1] The facility, completed in 2021, is a two-floor office building with a total net floor area of 2,366 m^2. Using real-time data from the building and a 300 s sampling time h, we determined loss and efficiency factors of the state-space model (12) to be

$$\alpha_1 = 0.99947,\ \alpha_2 = 0.999,\ \beta_1 = 0.075,$$
$$\beta_2 = 0.075,\ \beta_3 = 0.0833,\ \beta_4 = 0.0694,\ \beta_5 = 0.0942.$$

The 300 s sampling interval exceeds the minimum off and on periods required by the heat pumps, rendering dwell time considerations obsolete. At each time step k, we dynamically update the $COP_i(k)$ and power input $P_{\mathrm{HP},i}(k)$ for both heat pumps $i = 1, 2$. These updates are based on the supply temperature, derived from the current state of the hot water storage tank, and a constant brine temperature of 8 °C (281 K). As for forecasting within the current time step, we consider $COP_i(k+j|k)$ and $P_{\mathrm{HP},i}(k+j|k)$ as fixed values. This approach improves on the static COP assumption found in Löhr and Mönnigmann (2018). The heat output generated by a single activated heating rod, i.e., q_{HR_0}, is 9 kW. The capacity of the hot water storage tank is $E_{\mathrm{ST}}^{\max} = 72.48$ kWh, operating within a temperature range of 23-65 °C (296-338 K), while the battery has a capacity of $E_{\mathrm{BT}}^{\max} = 35.1$ kWh with $\eta = 0.9$ for the battery inverter. Solar irradiance data, used to fit the linear model and determine $P_{\mathrm{PV}}(k)$ at each time step, is sourced from solcast. [2] We assume that precise forecasts for electrical and thermal loads are accessible at every time step for validation purposes. We use actual data recorded from the building for this purpose.

4.1 MPC parameters

Our primary goals include reducing grid dependency, prioritizing use of heat pumps over heating rods, and ensuring reference tracking for the storage tank and battery. Specifically, the tracking problem involves maintaining 50 % of the capacities of the storage tank and battery reserved for dynamic operation. Tuning parameters of the cost function (14) that are suitable for these purposes were determined by numerical experiments. They are given in Table 2.
All simulations are based on an arbitrarily chosen four-day period, which spans from March 15th to March 18th, 2023. For the system under study during this interval, the mean daily electrical load demand is 230 kWh, the mean daily thermal load demand is 484 kWh, and the mean daily solar irradiation is 190 kWh. All MIQP problems were solved using the CPLEX solver on a Core i5, 1.7 GHz processor.

4.2 Comparison metrics

We assess computational demands using t_{com}, the time required to solve (19). When we solve (19) repeatedly in

[1] AUDAX, Niedereimerfeld 47, 59823 Arnsberg, Germany
[2] https://solcast.com

Table 2. MPC tuning parameters

Parameter	Value	Impact
$r_{\mathrm{E,ST}}$, $r_{\mathrm{E,BT}}$	40	Reference tracking
$r_{\mathrm{BT,ch}}$, $r_{\mathrm{BT,dis}}$	1	Penalize battery energy flows
$r_{\mathrm{G,dem}}$, $r_{\mathrm{G,sup}}$	100	Penalize grid energy flows
r_{κ}, r_{λ}	5, 100	Penalize discrete energy flows

closed-loop simulations, we report the mean and maximum values, which are denoted by $t_{\mathrm{com}}^{\mathrm{mean}}$ and $t_{\mathrm{com}}^{\mathrm{max}}$, respectively. In addition to t_{com}, we use the closed-loop cost as a metric for comparing the MIQP and the mMIQP variants of our MPC algorithm. More precisely, let $V_{\mathrm{MPC}}(k)$ refer to the cost function value (18a) of the closed-loop optimal solution at time step k of the closed-loop simulation under consideration. Let $V_{\mathrm{MPC}}^{\mathrm{mean}}$ refer to the time-mean of these values for a simulation, i.e.,

$$V_{\mathrm{MPC}}^{\mathrm{mean}} = \frac{1}{L}\sum_{k=0}^{L-1} V_{\mathrm{MPC}}(k)$$

where L is the number of time steps carried out in the simulation.

4.3 mMIQP versus MIQP

The mMIQP problem replaces some of the integer inputs of the corresponding MIQP problem by real-valued inputs. Because this amounts to a relaxation of some of the constraints of MIQP, the mMIQP solution results in cost function value that is lower than or equal to the cost function for the corresponding MIQP. However, since we are altering the behaviour of the system by allowing predictions to violate the physically motivated integer constraints, we need to check if a recursively feasible solution results. While a theoretical investigation of the recursive feasibility is beyond the present paper, we analyse the feasibility properties in extensive numerical experiments.

Closed loop simulations We conduct closed-loop simulations for three scenarios: MIQP with $N = 33$, mMIQP with $N = 33$ and $i_s = 1$, and mMIQP with $N = 192$ and $i_s = 1$. Further analysis regarding the selection of i_s values will be presented later. It will be evident from the results discussed further below that $N = 33$ is the maximum horizon the MIQP can be solved for with the given computational resources.
It will also be evident that the horizon can be extended considerably to $N = 192$ for MPC with mMIQP and $i_s = 1$ (see section 3.4), while retaining recursive feasibility in all our computational experiments without considerable improvement in results from further extending the horizon.
For each scenario, the MIQP problem (19) was solved 1152 times by running closed-loop simulations, utilizing real data from the targeted four-day span. The closed-loop cost values V_{MPC} is shown in Fig. 2 for these 1152 solutions, where we used a moving average with 6 time steps to filter out high-frequency fluctuations.
A summary of results obtained with the comparison metrics introduced in Section 4.2 is presented in Table 3. This table states the average of the closed-loop cost values depicted in Fig. 2, the average computational time, and the maximum computational time required for a single iteration of solving MIQP (19).
In the following paragraphs, we will elaborate on the findings presented in Table 3 and Fig. 2.

Table 3. Comparative analysis of scenario solutions: computational time and $V_{\mathrm{MPC}}^{\mathrm{mean}}$ outcomes

Scenario \ Metrics	$V_{\mathrm{MPC}}^{\mathrm{mean}}$	$t_{\mathrm{com}}^{\mathrm{mean}}$(s)	$t_{\mathrm{com}}^{\mathrm{max}}$(s)
$\mathrm{MIQP}_{N=33}$	1.6905e4	14.43	432
$\mathrm{mMIQP}_{N=33}$	1.7801e4	0.0834	0.0891
$\mathrm{mMIQP}_{N=192}$	1.5753e4	3.19	11.34

Computational time assessment Considering the sampling time of 300 seconds, the implementation within the actual building requires that solving (19) should not exceed approximately 15 seconds. It is evident from Table 3 that a horizon of $N = 33$ for MIQP results in an average computation time that meets this requirement. However, it should be noted that actual computational times can occasionally exceed the 15-second limit, as indicated the $t_{\mathrm{com}}^{\mathrm{max}}$ value in Table 3. This implies that even $N = 33$ is an optimistic horizon length that would require the MPC-based controller to be augmented with a fallback control strategy, if the MPC controller was to be based on solving the MIQP problems.
The values of $t_{\mathrm{com}}^{\mathrm{mean}}$ and $t_{\mathrm{com}}^{\mathrm{max}}$ in Table 3 indicate that mMIQP leads to a significant reduction in computational effort compared to the original MIQP problem as expected. This reduction implies longer horizons than those achievable with standard MIQP can be used with mMIQP. Our computational experiments reveal that a horizon of $N = 192$ in mMIQP still results in a smaller computational effort than MIQP with $N = 33$.

Control performance assessment Figure 2 shows that the MIQP solution results in slightly better closed-loop cost function values $V_{\mathrm{MPC}}(k)$ than mMIQP, if MIQP and mMIQP are solved for the same horizon $N = 33$. Because it results in a drastic reduction of the computation time, longer horizons can be treated, however, with mMIQP. As indicated by the $V_{\mathrm{MPC}}^{\mathrm{mean}}$ values in Table 3, extending the horizon results in lower closed-loop cost values on average for mMIQP with $N = 192$ compared to MIQP with $N = 33$.
The observed variations in the values of $V_{\mathrm{MPC}}(k)$ across the scenarios, as depicted in Fig. 2, are largely attributed to the performance in regulating the battery levels, which are shown in Fig. 3. The performance of the controllers in managing thermal flows and storage tank levels is nearly identical across the three scenarios. We have excluded detailed presentations in figures for brevity here.
Figure 3 shows that mMIQP with a horizon of $N = 192$ achieves superior control performance in maintaining the battery near its target 50 % state of charge. Note this is achieved even though mMIQP with a horizon of $N = 192$ still requiring less computational time than MIQP with the shorter horizon $N = 33$.

Computational time/sub-optimality trade-off It remains to investigate the impact of the choice of i_s on computational times and control performance. We again solve MPC with mMQP 1152 times and vary i_s for this purpose. All remaining parameters are not altered, and the horizon is set to $N = 33$.
We consider the $V_{\mathrm{MPC}}^{\mathrm{mean}}$ value obtained in the case of standard MIQP to be the reference value in the comparison that follow. Let $\Delta V_{\mathrm{MPC}}^{\mathrm{mean}}$ be the difference between

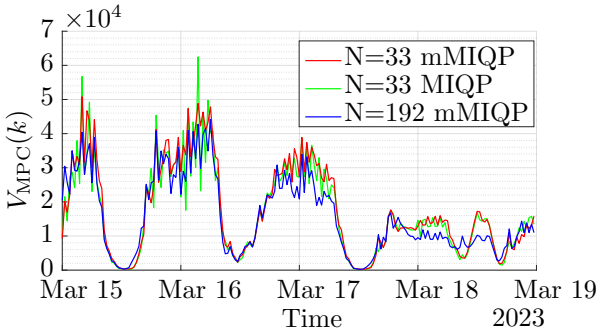

Fig. 2. Comparison of closed-loop cost $V_{\mathrm{MPC}}(k)$.

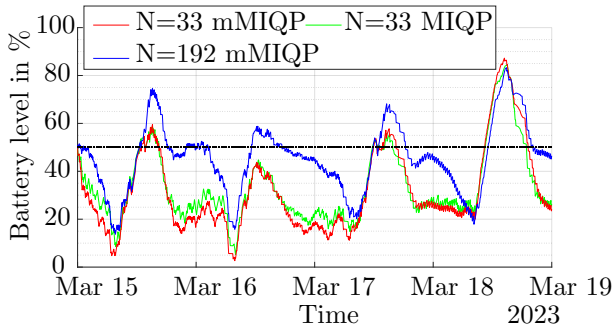

Fig. 3. Comparison of simulated battery levels. The dashed line represents the 50 % reference level.

the $V_{\mathrm{MPC}}^{\mathrm{mean}}$ value obtained from the mMIQP solution and this reference value. A larger value of $\Delta V_{\mathrm{MPC}}^{\mathrm{mean}}$ obviously indicates a larger level of suboptimality must be accepted. Figure 4 shows $\Delta V_{\mathrm{MPC}}^{\mathrm{mean}}$ for various values of i_s. Additionally, the figure reveals the relation of $\Delta V_{\mathrm{MPC}}^{\mathrm{mean}}$ to the average computation times $t_{\mathrm{comp}}^{\mathrm{mean}}$, showing how the choice of i_s results in a trade-off between suboptimality and computational efficiency. Notably, as i_s increases, there is

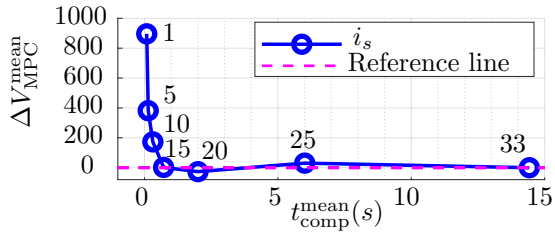

Fig. 4. Impact of i_s on $\Delta V_{\mathrm{MPC}}^{\mathrm{mean}}$ and $t_{\mathrm{comp}}^{\mathrm{mean}}$. Reference line set to 1.6905e4 is $V_{\mathrm{MPC}}^{\mathrm{mean}}$ for MIQP with $N = 33$.

an exponential growth in computational time. However, this increased computational effort does not correspond to a proportionate decrease in the sub-optimality of the solution, represented by $\Delta V_{\mathrm{MPC}}^{\mathrm{mean}}$. Figure 4 also shows that, even with i_s=1, the average of closed-loop cost values in the case of mMIQP, i.e., $V_{\mathrm{MPC}}^{\mathrm{mean}}$, is not significantly different from the reference line representing the solution of standard MIQP. However, there is a substantial reduction in computational time. The subtle yet better performance of $i_s = 20$ over $i_s = 33$ is linked to the same factor causing the variable trends seen in Fig. 2 between the MIQP and mMIQP (depicted by the green and red lines, respectively). In rare cases, the mMIQP outperformed the MIQP even with the same horizons.

Considering the computational resources, desired horizon, and system complexity, an effective compromise can be made in choosing i_s. This compromise seeks to lower computational time while still securing a near optimal performance, as seen with the selection of $i_s = 15$ for the described system.

5. CONCLUSION

In this study, we employed a hybrid MPC approach to optimize energy generation, consumption, and storage in office buildings. We introduced an auxiliary problem that relaxes integer constraints for later time points along the horizon, thereby significantly reducing computational effort. We evaluated the proposed method by conducting simulations using real world data from an office building. The results indicate that our approach can achieve near-optimal solutions while significantly reducing computational time rendering it highly practical for real-time applications.

ACKNOWLEDGEMENTS

We are grateful to our project partners at AUDAX, for providing access to their building. Also, we appreciate the support of our partners at ManageE and InTradeSys within the research project PraedNWG.

REFERENCES

Afram, A., Janabi-Sharifi, F., Fung, A.S., and Raahemifar, K. (2017). Artificial neural network (ANN) based model predictive control (MPC) and optimization of HVAC systems: A state of the art review and case study of a residential HVAC system. *Energy and Buildings*, 141, 96–113.

Aghemo, C., Virgone, J., Fracastoro, G.V., Pellegrino, A., Blaso, L., Savoyat, J., and Johannes, K. (2013). Management and monitoring of public buildings through ICT based systems: Control rules for energy saving with lighting and HVAC services. *Frontiers of Architectural Research*, 2(2), 147–161.

Axehill, D. and Hansson, A. (2006). A mixed integer dual quadratic programming algorithm tailored for MPC. In *Proceedings of the 45th IEEE Conference on Decision and Control*, 5693–5698. IEEE.

Cagienard, R., Grieder, P., Kerrigan, E., and Morari, M. (2007). Move blocking strategies in receding horizon control. *Journal of Process Control*, 17(6), 563–570. doi: https://doi.org/10.1016/j.jprocont.2007.01.001.

Killian, M. and Kozek, M. (2016). Ten questions concerning model predictive control for energy efficient buildings. *Building and Environment*, 105, 403–412.

Löhr, Y., Klauco, M., Fikar, M., and Mönnigmann, M. (2020). Machine Learning Assisted Solutions of Mixed Integer MPC on Embedded Platforms. *IFAC-PapersOnLine*, 53(2), 5195–5200. doi: https://doi.org/10.1016/j.ifacol.2020.12.1189. 21th IFAC World Congress.

Löhr, Y. and Mönnigmann, M. (2018). Optimal operation of electrical heating system with hybrid model predictive control. In *Proceedings of the 10th Symposium on Control of Power and Energy Systems (CPES2018)*, 274–279.

Löhr, Y. and Mönnigmann, M. (2021). MPC for heating systems with minimum up- and down-time requirements. *IFAC-PapersOnLine*, 54(6), 206–211. 7th IFAC Conference on Nonlinear Model Predictive Control 2021.

Maciejowski, J.M. and Huzmezan, M. (2007). Predictive control. In *Robust Flight Control: A Design Challenge*, 125–134. Springer.

Yao, Y. and Shekhar, D.K. (2021). State of the art review on model predictive control (MPC) in Heating Ventilation and Air-conditioning (HVAC) field. *Building and Environment*, 200, 107952.